WAPD-T-3054

Conf-950816--1

IRRADIATION-ASSISTED STRESS CORROSION CRACKING OF HTH ALLOY X-750 AND ALLOY 625

R. Bajaj, W. J. Mills, M. R. Lebo, B. Z. Hyatt, and M. G. Burke

U. S. Department of Energy Contract DE-AC11-93PN38195

BETTIS ATOMIC POWER LABORATORY WEST MIFFLIN, PENNSYLVANIA 15122-0079

Operated for the U.S. Department of Energy
by WESTINGHOUSE ELECTRIC CORPORATION

DISCLAIMER

Portions of this document may be illegible in electronic image products. Images are produced from the best available original document.

Irradiation-Assisted Stress Corrosion Cracking of HTH Alloy X-750 and Alloy 625

R. Bajaj, W. J. Mills, M. R. Lebo, B. Z. Hyatt and M. G. Burke
Bettis Atomic Power Laboratory
Westinghouse Electric Corporation
West Mifflin, Pennsylvania 15122

Abstract

In-reactor testing of bolt-loaded compact tension specimens was performed in 360°C water to determine the irradiation-assisted stress corrosion cracking (IASCC) behavior of HTH Alloy X-750 and direct-aged Alloy 625. New data confirm previous results showing that high irradiation levels reduce SCC resistance in Alloy X-750. Heat-to-heat variability correlates with boron content, with low boron heats showing improved IASCC properties. Alloy 625 is resistant to IASCC, as no cracking was observed in any Alloy 625 specimens.

Microstructural, microchemical and deformation studies were performed to characterize the mechanisms responsible for IASCC in Alloy X-750 and the lack of an effect in Alloy 625. The mechanisms under investigation are: boron transmutation effects, radiation-induced changes in microstructure and deformation characteristics, and radiation-induced segregation. Irradiation of Alloy X-750 caused significant strengthening and ductility loss that was associated with the formation of cavities and dislocation loops. High irradiation levels did not cause significant segregation of alloying or trace elements in Alloy X-750. Irradiation of Alloy 625 resulted in the formation of small dislocation loops and a fine body-centered-orthorhombic phase. The strengthening due to the loops and precipitates was apparently offset by a partial dissolution of γ" precipitates, as Alloy 625 showed no irradiation-induced strengthening or ductility loss.

In the nonirradiated condition, an IASCC susceptible HTH heat containing 28 ppm B showed grain boundary segregation of boron, whereas a nonsusceptible HTH heat containing 2 ppm B and Alloy 625 with 20 ppm B did not show significant boron segregation. To determine the distribution of transmutation-produced helium, these alloys were annealed at 816°C after irradiation to agglomerate the helium. Helium bubbles were observed at grain boundaries in the high boron HTH heat, but little or no evidence of grain boundary helium was observed in the low boron HTH heat and Alloy 625. Based on these results, transmutation of boron to helium at grain boundaries, coupled with matrix strengthening, is believed to be responsible for IASCC in Alloy X-750, and the absence of these two effects results in the superior IASCC resistance displayed by Alloy 625.

Key terms: irradiation-assisted stress corrosion cracking, HTH Alloy X-750, Alloy 625, boron-to-helium transmutation, radiation strengthening, radiation-induced segregation

Introduction

Alloy X-750 is a nickel-base superalloy that is used as a fastener material in light water reactors (LWR) as a result of its strength, load relaxation resistance and corrosion resistance. Environmental testing has revealed, however, that it is susceptible to intergranular stress corrosion cracking (SCC) in water,[1,2] and SCC of Alloy X-750 LWR components has been observed.[3,4] In-reactor[5,6] and postirradiation (performed at Knolls Atomic Power Laboratory and cited in Reference 6) SCC testing have also shown that this material is susceptible to irradiation-assisted SCC (IASCC). Direct-aged Alloy 625, with strength levels comparable to those for Alloy X-750, shows promise for high strength fastener applications due to its superior SCC resistance in the nonirradiated and irradiated conditions.[5] The primary objective of this study is to investigate the mechanisms responsible for IASCC in Alloy X-750 and the lack of an irradiation effect in Alloy 625.

In-reactor SCC testing of precracked Alloy X-750 specimens[5] showed that irradiation to fluences above 10^{19} n/cm^2 (E > 1 MeV) can degrade SCC performance. Heat-to-heat variations in IASCC susceptibility for HTH materials correlated with differences in boron content.[5,6] Heats with less than 10 ppm boron showed little or no effect, whereas those with high boron showed substantial degradation. Reference 5 also reported no evidence of SCC in any Alloy 625 specimens, even though they were highly loaded and irradiated up to

4.4 x 10^{20} n/cm^2. In-reactor swelling mandrel tests performed in pressurized and boiling water reactor (PWR and BWR) environments[7,8] showed SCC at diametral strains less than 1% for both Alloy X-750 and cold worked and aged Alloy 625 at fluences above 10^{21} n/cm^2. Alloy 625 was equal or superior to Alloy X-750 in PWR water, while Alloy X-750 outperformed Alloy 625 in BWR water. Note that the loading conditions and heat treatments used in the swelling mandrel tests were different from those used in this study.

This study characterizes the in-reactor SCC behavior of precracked HTH Alloy X-750 and Alloy 625 specimens over a wide range of fluences and loading conditions. Emphasis was placed on testing at lower stress intensity factors (K_I) and longer exposure times, relative to Reference 1. In addition, detailed microstructural, microchemical and deformation studies were performed to characterize irradiation effects in both alloys. The mechanisms under investigation include boron transmutation effects, radiation effects on microstructure and deformation characteristics, and radiation-induced segregation (RIS). Specifically, analytical electron microscopy (AEM) methods, including microanalysis using a conventional scanning transmission electron microscope with an energy dispersive X-ray spectrometer (STEM-EDS), were used to evaluate radiation-induced microstructural changes and transmutation effects in susceptible and nonsusceptible heats of Alloy X-750 and a representative heat of Alloy 625. RIS studies were performed on an SCC susceptible heat of Alloy X-750 using a field emission gun STEM equipped with parallel electron energy loss spectrometer and electron dispersive X-ray spectrometer (FEG/STEM/PEELS+EDS) with a spatial resolution capability of ~2 nm. The role of strengthening was characterized by postirradiation tension testing of both materials.

Experimental Procedures

Two types of Condition HTH Alloy X-750 were included in this study: process variation heats (Heats A1-A6) where metal producers attempted to optimize SCC properties by controlling trace elements and thermomechanical processing methods, and original process heats (A7-A11 and B1) that were conventionally melted and processed. Alloy 625 heats were aged at 663°C for 80 hours. The chemical composition and mechanical properties for the test materials are provided in References 5 and 6. Alloy 625 Heat B3, which was not studied previously, had 62.5% Ni, 21.8% Cr, 8.8% Mo, 2.3% Fe, 0.04% C and 18 ppm B. The mean grain diameter was nominally 100-120 μm for HTH Alloy X-750 heats and 10-20 μm for Alloy 625 heats.

SCC tests were performed on bolt-loaded compact tension (CT) specimens with a width of 20.3 mm and a thickness of 10.2 mm that were precracked prior to irradiation. Specimens were exposed to water containing 40 to 60 cc H_2/kg H_2O in both in-flux and out-of-flux locations. The irradiation temperature was 360°C. The room temperature pH of the water was between 10.1 and 10.3, the oxygen content was less than 40 ppb, and the conductivity of the water was between 30 and 50 μS/cm. After irradiation, the final residual bolt load was measured, and the specimens were broken apart so the fracture surfaces could be examined visually and with an SEM to determine the extent of SCC. Details concerning irradiation conditions, specimen loading and unloading methods, and destructive evaluations are provided in Reference 5.

Tension tests were conducted on flat tension specimens with a gage length of 19 mm, which were irradiated at 264°C to a fluence of 2.4 x 10^{20} n/cm^2 (E>1 MeV). Tests were conducted in air at 66° and 288°C at a strain rate of 2.2 x 10^{-5} s^{-1}. Fracture surfaces were examined using an SEM.

The microstructure of the nonirradiated and irradiated (fluence = 2.3 x 10^{20} n/cm^2 at nominally 360°C) alloys was characterized by conventional AEM techniques. Thin-foil specimens were prepared from 3-mm diameter pins by standard electropolishing techniques using an electrolyte of 20% $HClO_4$ - 80% CH_3OH at -40°C. Microstructural characterization was performed using a Philips CM12 analytical electron microscope operated at 120 kV, and equipped with a LaB_6 cathode (nominal probe size of ~7 nm) and a Link Analytical LZ5 windowless energy dispersive x-ray spectrometer and an AN10/85S analyzer.

FEG/STEM/PEELS+EDS analyses were performed on one IASCC sensitive heat (HTH Heat A1) of Alloy X-750 in both the nonirradiated and irradiated conditions to evaluate if RIS was responsible for the observed degradation in IASCC resistance. Selected foils <50 nm in thickness were analyzed in a Philips EM400T/FEG, equipped with a Gatan 666 PEELS and an EDAX 9100/70 EDS system, operated in the STEM

mode. Based on Monte Carlo calculations of electron scattering in nickel, the spatial resolution for X-ray microanalysis was estimated as ~6 nm at a foil thickness of ~50 nm.

To evaluate the effects of boron transmutation, slices cut from the pin specimens were heat treated at 816°C for 1 hour to agglomerate the helium into bubbles resolvable in an AEM. This annealing condition was selected to allow some helium agglomeration while avoiding extensive diffusion. Calculations based on vacancy diffusion[9] and helium annealing studies[10] both indicate that the diffusion distance is about 0.25 μm which is two to three orders of magnitude smaller than the grain size and an order of magnitude smaller than the helium recoil distance, as discussed later. Bubbles were imaged using both kinematic and under focus conditions.

Results and Discussion

SCC Performance

All in-reactor SCC results for process variation and original process HTH Alloy X-750 heats are summarized in Figure 1, in which the amount of crack extension (represented by fullness of symbols) is plotted as a function of fluence and initial K_I. The new data support the conclusions in Reference 5 that irradiation to fluences greater than 10^{19} n/cm^2 significantly reduces high temperature SCC resistance, as illustrated by the increased number of filled symbols at high fluences. The amount of SCC in low fluence (10^{14} to 10^{18} n/cm^2) specimens was typically twice that for out-of-flux specimens, but only half that for highly irradiated specimens. In this regime, radiolysis effects are believed to be responsible for the modest reduction in SCC resistance, because the low neutron exposures are unlikely to alter the microstructure significantly.

Figure 1b shows that the low boron heats (Heats A7-A9) were not susceptible to IASCC. In fact, none of the irradiated specimens from these heats exhibited any high temperature SCC, despite being highly stressed and irradiated. The high boron original process heats (Heats A10, A11 and B1) with more than 40 ppm boron, and process variation heats with 20 to 30 ppm boron showed extensive IASCC under comparable and less severe irradiation and K_I conditions. As discussed in Reference 5, these findings indicate that boron content is responsible for heat-to-heat variability. Figure 2, in which the amount of SCC is plotted as a function of boron content for highly irradiated specimens, shows a threshold for IASCC susceptibility between 10 and 20 ppm boron. Heats with less than 10 ppm boron showed no SCC, while those with more than 20 ppm boron showed extensive cracking. Once the threshold was exceeded, further increases in boron content are seen to have little additional effect. Boron is generally considered to be a beneficial trace element because it improves the hot working behavior and creep properties of nickel-base superalloys.[11-13] Moreover, autoclave testing[14] has demonstrated that boron is beneficial to the high temperature SCC performance of nonirradiated Alloy X-750, but the current in-reactor results show an adverse effect of high boron levels on IASCC resistance. The details of this embrittling mechanism will be discussed later.

Figure 3, which compares the IASCC resistance for HTH Alloy X-750 and Alloy 625, shows no evidence of SCC in any Alloy 625 specimens even though they were highly loaded (up to 82 MPa$\sqrt{m}$) and highly irradiated (up to 4.4 x 10^{20} n/cm^2). Under comparable irradiation conditions, extensive SCC was observed in HTH Alloy X-750 at K_I levels as low as 30 to 40 MPa$\sqrt{m}$. This comparison shows that Alloy 625 is clearly superior to HTH Alloy X-750 for in-reactor applications with significant neutron exposure.

Tensile Properties and Fractography of Alloys X-750 and 625

Tensile properties for Alloy X-750 and Alloy 625 in both the nonirradiated and irradiated conditions were characterized in 66° and 288°C air. The same pre- and postirradiation trends were observed at both temperatures, and the 288°C results are shown in Figure 4. For Alloy X-750, irradiation caused a 33 to 45% increase in yield strength (YS) and essentially no change in ultimate strength (UTS). A significant decrease in total elongation occurred in all heats with Heat A10 showing the most dramatic decrease. While there was little heat-to-heat variability in pre- and postirradiation strength levels, variations in elongation were observed with Heat A10 exhibiting the lowest ductility, especially after irradiation.

Fractographic examination of HTH heats in the nonirradiated condition showed a mixed transgranular/intergranular fracture mode with secondary cracking. Heat A10 exhibited the most intergranular fracture. The

transgranular areas showed dimples or void sheets and the intergranular regions showed fine dimples on the fractured grain facets. Irradiation resulted in an increase in intergranularity of the fracture and rather poorly defined and shallow dimples. The grain facets also showed dimples but they were shallower than those in the nonirradiated condition indicating increased planar slip. In addition, the irradiated specimens showed evidence of channel fracture at both temperatures, which also indicates that irradiation promotes planar slip.

In contrast to Alloy X-750, irradiation did not result in an increase in YS for Alloy 625, as shown in Figure 4. In fact, two of the three heats examined showed a reduction in YS. Irradiation also resulted in a decrease in UTS and an increase in total elongation in all heats. The strain hardening capability of Alloy 625 was essentially unaffected by irradiation.

Irradiation had no effect on the fracture morphology of Alloy 625. Heats A12 and D1 with typical fine grain microstructures showed fully ductile dimpled fractures which were essentially unaffected by irradiation. Heat B3 had duplex grain structure and exhibited a mixed transgranular/intergranular failure mode with the larger grains showing intergranular fracture in both the nonirradiated and irradiated conditions.

Microstructural Analysis: HTH Alloy X-750

The nonirradiated Alloy X-750 materials were characterized by the presence of a uniform distribution of intragranular cuboidal γ' precipitates, with an average size of 16 nm. These alloys exhibited extensive intergranular carbide precipitation, with the Cr-rich $M_{23}C_6$ as the dominant carbide. In addition, M_7C_3 and a few thin TiNb(CN) films were observed in both the high and low boron heats. High boron HTH Heat A1 also exhibited another intergranular precipitate identified by conventional STEM-EDS and FEG/STEM/PEELS+EDS microanalyses as nickel and boron-rich $M_{23}X_6$. This fcc precipitate contained a pronounced defect substructure and exhibited a slightly mottled appearance. The grain boundaries and carbides acted as preferential sites for γ' precipitation during the HTH heat treatment. Figure 5a shows the extent and morphology of γ' precipitates near and away from a grain boundary. Note the considerably coarser γ' precipitates located both at the boundary and at intergranular carbides. The secondary electron image in Figure 5b shows the general extent of intergranular carbide precipitation in Heat A1. STEM-EDS microanalysis of grain boundary regions revealed some narrow zones (<100 nm) which were depleted in Cr. The minimum measured Cr content, corrected for γ', was $\sim$13 wt%.

Neutron irradiation promoted extensive damage throughout the microstructure, as evidenced by the complex matrix contrast observed in the bright field micrograph in Figure 6. Figure 6 also contains an example of the intergranular agglomerated Cr-rich $M_{23}C_6$/Ni,B-rich $M_{23}X_6$ precipitates present in Heat A1. The irradiation-induced damage consisted of fine ($\sim$5 nm) cavities throughout the matrix and the formation of fine faulted dislocation loops which were confined to the γ' precipitates. Examples of the fine cavities and loops are shown in Figure 7. Annealing the irradiated material at 816°C annihilated the 5 nm cavities in both heats, thereby demonstrating that they were irradiation-induced voids. This is in agreement with Porter[15] who showed that the equivalent heat treatment in 304L stainless steel irradiated to 5 x 10^{22} n/cm^2 at 415°C reduced the void number density by two orders of magnitude.

The results of conventional STEM-EDS studies showed that neutron irradiation did not promote significant long range segregation or depletion in Heats A1 or A7. Microchemical analysis of short range segregation, by FEG/STEM/PEELS+EDS, of irradiated HTH Heat A1 showed only a slight (2-2.5 wt% corrected for γ') depletion of Cr in the grain and phase boundaries. Some boundaries in irradiated Heat A1 (0.07% bulk Si) showed a very slight increase in silicon concentration to 0.3 wt%, but this is probably not significant since the detectable minimum mass fraction limit is also about 0.3 wt%. Moreover, two low-boron heats with high bulk silicon contents (Heats A8 and A9 with 0.09 and 0.06% Si) were not susceptible to IASCC, indicating that there is no correlation between silicon and IASCC resistance. Irradiation did not cause additional segregation of phosphorus or sulfur to the grain boundaries.

Microstructural Analysis: Alloy 625

AEM examination of this fine-grained material revealed the presence of a uniform distribution of fine ($\sim$15 nm diameter) intragranular disc-shaped γ" precipitates, which significantly strengthen the matrix. The extent

of intergranular carbide precipitation in this alloy was limited, with approximately 50% of the grain boundaries free of carbides. The dominant carbide observed in this alloy was Cr-rich $M_{23}C_6$, with lesser amounts of M_7C_3 and NbTi(CN). Coarse NbTi(CN) inclusions were observed to pin grain boundaries. The NbTi-rich carbonitrides were associated with irregular γ" precipitate free zones (PFZ). The variation in γ" size in the vicinity of a PFZ associated with a carbonitride inclusion is shown in the γ" precipitate dark-field transmission electron micrograph in Figure 8a. The limited extent of intergranular carbide precipitation is evident in the secondary electron micrograph in Figure 8b. STEM-EDS microanalysis of grain boundary regions showed no intergranular solute depletion or segregation.

Neutron irradiation of this alloy promoted the formation of "black spots" and fine (5 to 10 nm) dislocation loops, as shown in Figure 9a. More detailed examination of the irradiated material revealed the presence of a new precipitate phase approximately 5 nm in size, Figure 9b. Electron diffraction patterns indicated that this new phase was consistent with a body-centered-orthorhombic (bco) Pt_2Mo-type structure,[16,17] and has tentatively been identified as $Ni_2(NbMo)$. The average diameter of the γ" precipitates in this irradiated specimen was ~8 nm which suggests that these precipitates are partially dissolving during neutron irradiation. The lack of an effect of irradiation on Alloy 625 tensile properties indicates that the strengthening associated with the black spots, dislocation loops and $Ni_2(Nb,Mo)$ precipitates is offset by the reduction in strength associated with the partial dissolution of γ" precipitates. Conventional STEM-EDS microanalysis of grain boundary regions showed no intergranular solute depletion or segregation in the irradiated specimens.

Investigation of the Boron Transmutation Effects in Alloys X-750 and 625

Extensive studies have been performed to understand the apparent role of boron on IASCC. Detrimental effects of boron are usually associated with irradiation-induced helium embrittlement, where helium results primarily from the $B^{10}(n,\alpha)Li^7$ transmutation reaction with thermal neutrons. Thermal flux analysis revealed that approximately 50% of the B^{10} originally present is transmuted to helium at an equivalent fluence of 2 x 10^{20} n/cm^2 (E>1 MeV), where substantial IASCC was observed. Since B^{10} comprises about 20% of the total boron content, approximately 10% of the total boron is transmuted to helium.

Helium embrittlement, which is known to occur in iron-base[18] and nickel-base[19] alloys above 550°C, may also be operative in irradiated Alloy X-750 at lower temperatures where it is susceptible to intergranular SCC. Mechanisms of embrittlement due to lithium, another product of $B^{10}(n,\alpha)Li^7$ reaction, are not well understood. For example, liquid metal embrittlement and weakening of metallic bonds at the grain boundaries due to electronic charge transfer to segregated impurity atoms were discounted.[20-22] Effects of lithium on restructuring grain boundaries and on local chemical environment in water are noteworthy, but remain unproven. The current work focuses on helium as the embrittling species.

Secondary ion mass spectroscopy (SIMS) examinations of polished surfaces from susceptible and nonsusceptible Alloy X-750 heats and a typical Alloy 625 heat were conducted to determine the distribution of boron prior to irradiation. Results in Figure 10a show that HTH Heat A1 exhibited high concentrations of boron in the grain boundary regions. In low boron HTH Heat A7 and Alloy 625 Heat A12, the grain boundary regions did not reveal a high concentration of boron, as shown in Figures 10b and 10c, respectively.

Transmission electron microscopy (TEM) studies were performed on irradiated and 816°C annealed heats to determine the helium distribution developed during irradiation, and the results are shown in Figure 11. High boron (28 ppm) HTH Heat A1 had a heterogeneous distribution of helium bubbles, with the highest density occurring at grain boundaries and carbide/matrix interfaces (average bubble size was ~2 nm). This provides indirect evidence of helium in the grain boundary regions. Very few bubbles were observed in the grain interior and they were preferentially located on dislocations. In low boron (2 ppm) Heat A7 and Alloy 625 Heat A12 (20 ppm B), bubbles were very sparse in the grain boundaries, carbide/matrix interfaces and grain interior, as shown in Figure 11b and 11c, respectively. A few bubbles can be seen on dislocations. Bubbles in the matrix are believed to be due to helium transmutation from nickel via a two-step reaction: $Ni^{58}(n,\gamma)Ni^{59}$ followed by $Ni^{59}(n,\alpha)Fe^{56}$.

It has been suggested that the transmutation-produced helium ends up distributed away from the grain boundaries because of recoil with a recoil distance of 2 μm. Rowcliffe et al.[23] showed this not to be the case. Assuming that helium is formed within a 2 μm radius spherical shell surrounding each boron containing carbide or boron-rich area, they showed that the helium would be preferentially located at high angle boundaries because helium atoms reaching a grain boundary surface by recoil and by random diffusion are likely to remain on the boundary. Also, during irradiation the flow of vacancies is towards the sinks (grain boundaries, carbide/matrix interfaces) which would result in higher probability of helium/vacancy complex formation and mobility towards the sinks. Encounters between helium atoms would then be more frequent since their random walk would now be confined to the grain boundary plane and because of higher grain boundary diffusivity than lattice diffusivity.

The presence of grain boundary helium was demonstrated experimentally by Clausing and Bloom[24] in highly irradiated 304 stainless steel and by Sklad et al.[25] in Nimonic PE16 when specimens fractured intergranularly. The helium release corresponded to about 0.03 helium atoms per atom of grain boundary. This concentration is many orders of magnitude higher than the bulk concentration, thereby demonstrating that grain boundaries can contain a high concentration of helium transmuted from boron.

Helium is known to embrittle grain boundaries, and modeling work by Baskes[26] showed that the fracture stress can be reduced by an order of magnitude by the presence of small helium-vacancy complexes. It was suggested that each helium atom acts as a crack nucleus that enhances the fracture process. It was also surmised that helium strongly bonds to grain boundaries and that in essence a single helium atom causes a restructuring of the grain boundary, which lowers grain boundary cohesive strength.

Summary of IASCC Mechanisms

The IASCC susceptibility displayed by high boron HTH heats is associated with a boron-transmutation phenomenon coupled with irradiation-induced strengthening of the matrix and a tendency toward planar slip after irradiation. It is believed that transmutation-produced helium weakens the grain boundaries and thereby promotes intergranular SCC in water. The high strength matrix and tendency for planar slip increases strain concentrations at grain boundaries, which also contributes to decreased in-reactor SCC resistance.

The absence of helium bubbles in the irradiated low boron HTH heat after 816°C annealing coupled with the superior IASCC resistance displayed by low boron heats indicate that insufficient quantities of helium are generated to reduce grain boundary cohesive strength. It is noteworthy that this heat showed the same degree of strengthening as the high boron heats that were susceptible to IASCC. This indicates that the role of helium embrittlement is far more important than matrix strengthening.

The absence of helium embrittlement and matrix strengthening in Alloy 625 results in its virtual immunity to IASCC. Although Alloy 625 contained about 20 ppm boron, it showed much lower grain boundary enrichment levels than HTH Alloy X-750 heats with the same bulk levels. While boron enrichment may occur in Alloy 625, its greater grain boundary area, due to the small grain size, results in lower concentrations. The annealing studies clearly show that grain boundary helium levels in irradiated Alloy 625 were much lower than in its high boron HTH counterpart. The lack of matrix strengthening resulted from partial dissolution of γ" precipitates counteracting the strengthening effects of irradiation-induced lattice defects and $Ni_2(Nb,Mo)$ precipitates.

Conclusions

In-reactor SCC testing of bolt-loaded CT specimens was performed to characterize the IASCC properties of HTH Alloy X-750 and Alloy 625. Detailed microstructural and microchemical evaluations and postirradiation tension testing were also performed to establish IASCC mechanisms. The conclusions are provided below.

1. At fluences above 10^{19} n/cm^2, the in-reactor SCC resistance of HTH Alloy X-750 was significantly reduced. At low fluences (10^{14} to 10^{18} n/cm^2), there was only a slight degradation in SCC resistance that was attributed to radiolysis effects.

2. Heat-to-heat variability for HTH Alloy X-750 correlated with boron content. Heats with less than 10 ppm boron showed no IASCC, whereas those with more than 20 ppm boron showed a substantial degradation in SCC performance. Helium embrittlement of grain boundaries, resulting from the $B^{10}(n,\alpha)Li^7$ transmutation reaction, is believed to be responsible for the IASCC susceptibility displayed by high boron HTH heats.

3. Irradiation strengthening associated with the formation of dislocation loops and cavities was less important than helium embrittlement in increasing IASCC susceptibility of HTH Alloy X-750, because the resistant heats with low boron showed the same degree of strengthening as the susceptible high boron heats.

4. Irradiation caused only a slight (2-2.5 wt%) depletion of Cr at grain and phase boundaries and no significant increase in P, S or Si. As a result, radiation-induced segregation did not appear to contribute to IASCC.

5. The virtual immunity to IASCC displayed by Alloy 625 demonstrates that it is clearly superior to HTH Alloy X-750 for highly irradiated PWR applications. Irradiation neither strengthened the matrix nor generated significant helium enrichment at grain boundaries, which accounts for its superior resistance.

Acknowledgment

This work was performed under U. S. Department of Energy Contract DE-AC11-93PN38195 with Bettis Atomic Power Laboratory, a unit of Westinghouse Electric Corporation. Appreciation is extended to R. C. Hoffman, R. F. Luther and G. B. Sykes of Bettis for assisting with the irradiation experiments. Acknowledgments are also due to J. Greggi and J. J. Haugh of Westinghouse Science and Technology Center for AEM assistance, V. Sowle and K. Roarty-Dansfield of Knolls Atomic Power Laboratory for tension testing and E. A. Kenik of the Oak Ridge National Laboratory for FEG/STEM/PEELS+EDS investigation.

References

1. C. A. Grove and L. D. Petzold, Journal of Materials for Energy Systems, 7 (1985): p. 147.
2. I. L. W. Wilson and T. R. Mager, Corrosion, 42 (1986): p. 352.
3. A. A. Stein, "Proceedings: 1986 Workshop on Advanced High-Strength Materials," EPRI Report NP-6363, Edited by M. S. Gennaro and J. L. Nelson, May 1989.
3 4. A. R. McIlree, International Symposium on Environmental Degradation of Materials in Nuclear Power Systems-Water Reactors, (NACE, 1983), p. 838.
5. W. J. Mills, M. R. Lebo, J. J. Kearns, R. C. Hoffman, J. J. Korinko, R. F. Luther and G. B. Sykes, Sixth International Symposium on Environmental Degradation of Materials in Nuclear Power Systems - Water Reactors, (TMS, 1993), p. 633.
6. W. J. Mills, M. R. Lebo, R. Bajaj, J. J. Kearns, R. C. Hoffman and J. J. Korinko, "Irradiation Assisted Stress Corrosion Cracking of HTH Alloy X-750 and Alloy 625," Bettis Report WAPD-T-3034, March 1994.
7. F. Garzarolli, D. Alter, P. Dewes and J. L. Nelson, Third International Symposium on Environmental Degradation of Materials in Nuclear Power Systems-Water Reactors (TMS, 1988), p. 657.
8. F. Garzarolli, D. Alter and P. Dewes, Second International Symposium on Environmental Degradation of Materials in Nuclear Power Systems - Water Reactors, (ANS, 1986), p. 131.
9. Smithells Metals Reference Book, (Butterworths 1983), p. 13-11.
10. V. Philipps, K. Sonnenberg and J. M. Williams, Journal of Nuclear Materials, 107 (1982): p. 271.
11. E. E. Brown and D. R. Muzyka, Superalloys II, (John Wiley & Sons, 1987), p. 165.
12. R. T. Holt and W. Wallace, International Metals Reviews, Review 203, (1976): p. 1.
13. E. W. Ross and C. T. Sims, Superalloys II, (John Wiley & Sons, 1987), p. 97.
14. C. Benhamou, J. Daret and J. C. Van Duysen, Contribution des Expertises sur Materiaux a la Resolution des Problemes Rencontres dans les REP, Vol. 1, (SFEN, Paris, 1990), p. 30.

15. D. L. Porter, G. L. McVay and L. C. Walters, Effects of Radiation on Materials, ASTM STP 725 (1981): p. 500.
16. T. Saburi, K. Komatsu, M. Yamamoto, S. Nenno, and Y. Mituzani, Trans. TMS-AIME, 245 (1969): p. 2348.
17. S. K. Das and G. Thomas, Physica Status Solidi (a), 21 (1974): p. 177.
18. E. E. Bloom, Radiation Damage in Metals, (ASM, 1975): p. 295.
19. R. P. Shogan, "Neutron Irradiation Effects on the Tensile Properties of Inconel 718, Waspaloy and A286," Westinghouse Electric Corporation, WANL-TME-2791, 1971.
20. S. P. Lynch, Materials Science Forum, 46 (1989): p. 1.
21. C. L. Briant, Metallurgical Transactions, 21A (1990): p. 2339.
22. R. M. Boothby, Journal of Nuclear Materials, 186 (1992): p. 209.
23. A. F. Rowcliffe, G. J. C. Carpenter, H. F. Merrick and R. B. Nicholson, The Effects of Radiation on Structural Materials, ASTM STP 426 (1967): p. 161.
24. R. E. Clausing and E. E. Bloom, Grain Boundaries in Engineering Materials, (Claitor's, 1975): p. 491.
25. P. S. Sklad, R. E. Clausing and E. E. Bloom, Irradiation Effects on the Microstructure and Properties of Metals, ASTM STP 611 (1976): p. 139.
26. M. I. Baskes, "Recent Advances in Understanding Helium Embrittlement in Metals," Sandia National Laboratory Report, SAND 86-8816, 1986.

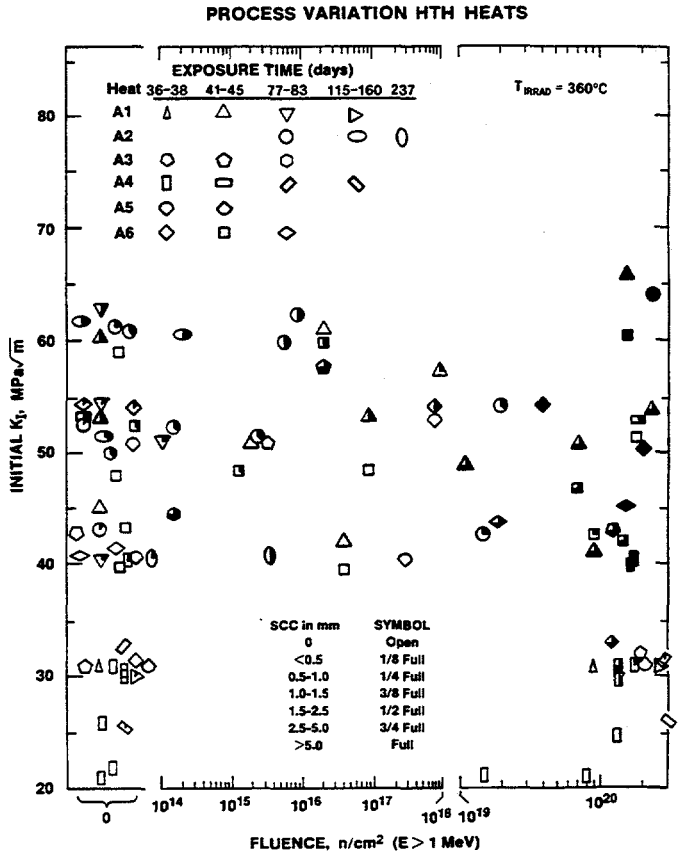

Figure 1a. Extent of SCC in process variation heats of HTH X-750 at various K_I and fluence levels.

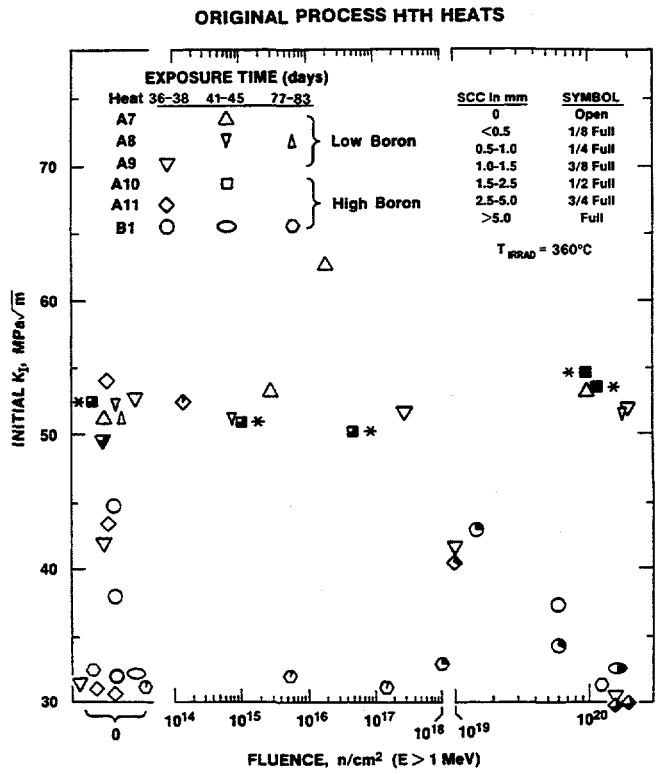

Figure 1b. Extent of SCC in original process heats of HTH X-750 at various K_I and fluence levels. Asterisks indicate that low temperature cracking may have occurred.

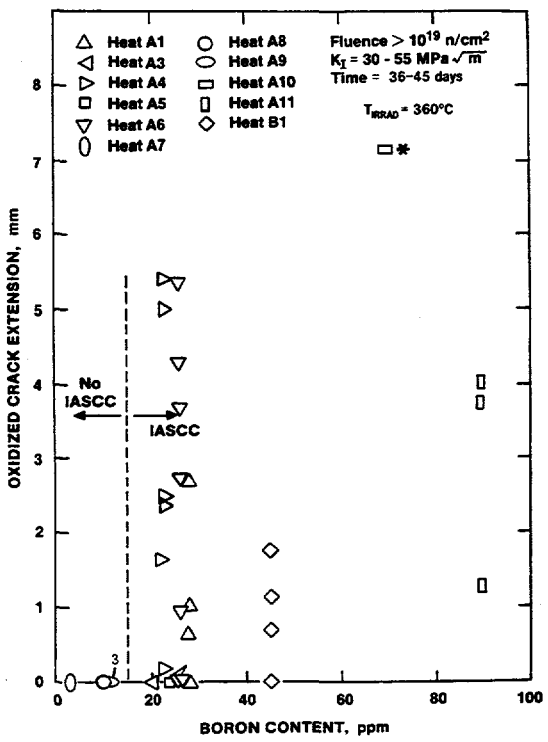

Figure 2. Extent of IASCC in HTH heats with various boron contents. Asterisk indicates that low temperature cracking may have occurred.

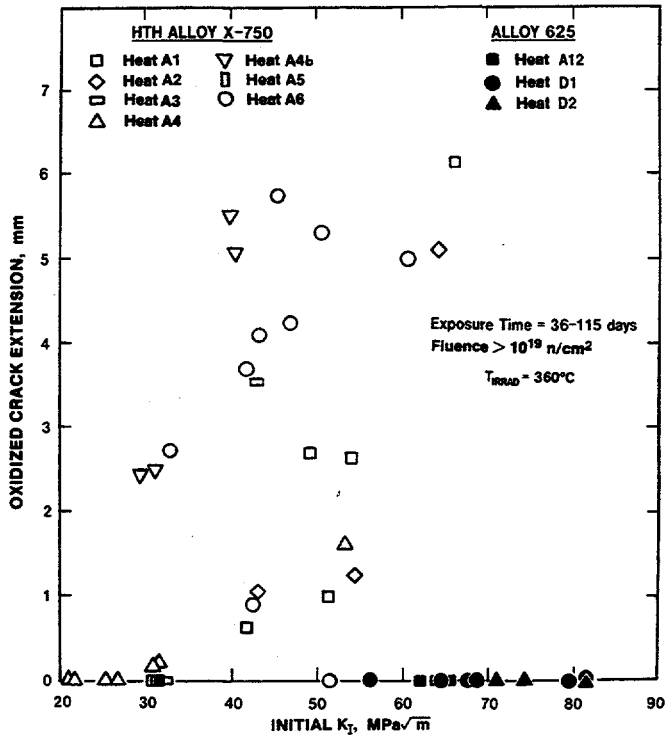

Figure 3. Extent of IASCC for process variation heats of HTH X-750 and Alloy 625 as a function of initial K_I.

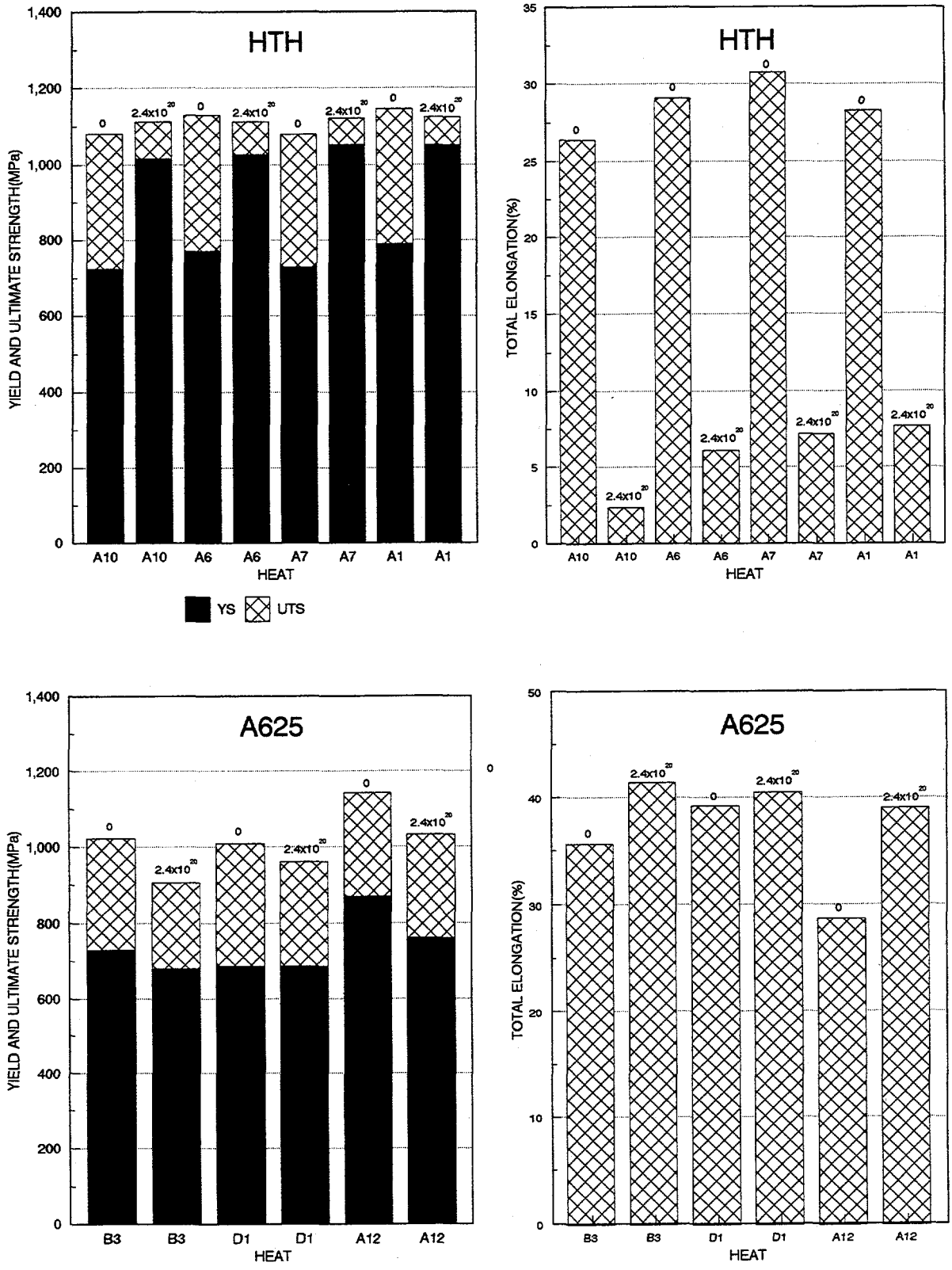

Figure 4. Tensile properties of nonirradiated and irradiated (at 264°C) HTH Alloy X-750 and Alloy 625 tested at 288°C. Fluence (in n/cm^2) is indicated above each bar.

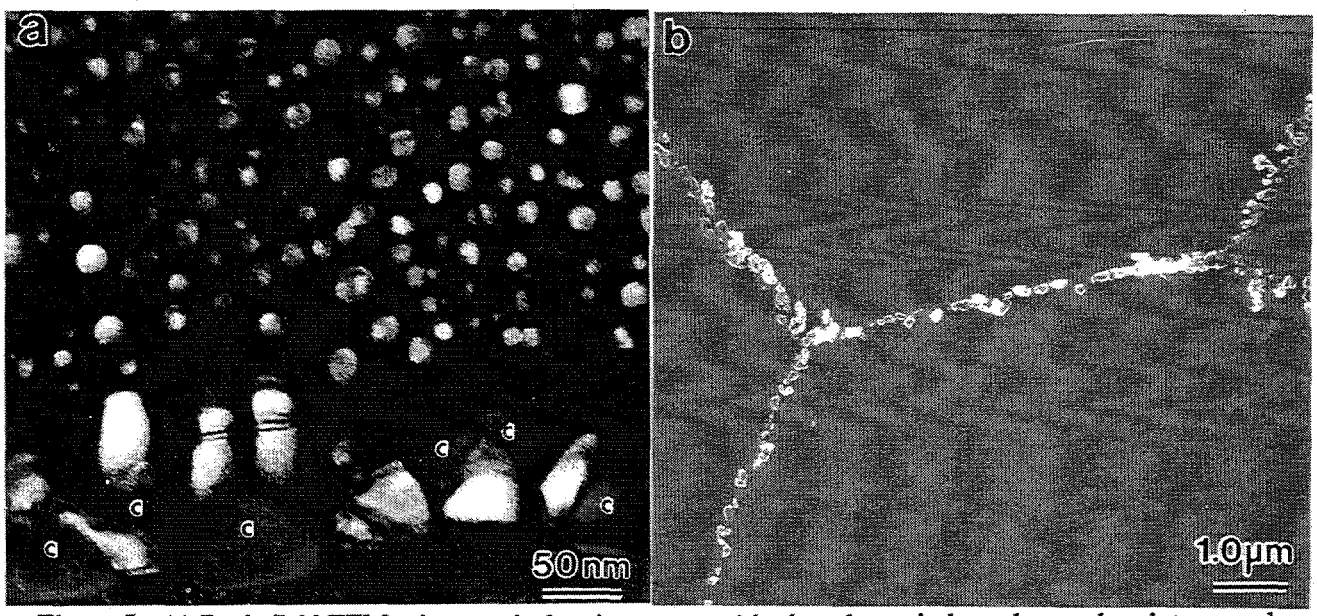

Figure 5. (a) Dark-field TEM micrograph showing coarse γ' both at the grain boundary and on intergranular carbides ("c"), and the fine intragranular γ' in Heat A7. (b) Secondary electron image showing the extent of intergranular carbide precipitation in HTH Alloy X-750, Heat A1.

Figure 6. TEM micrograph of irradiated Heat A1 with three complex intergranular Cr-rich $M_{23}C_6$ / Ni,B-rich $M_{23}X_6$ agglomerated precipitates (arrowed).

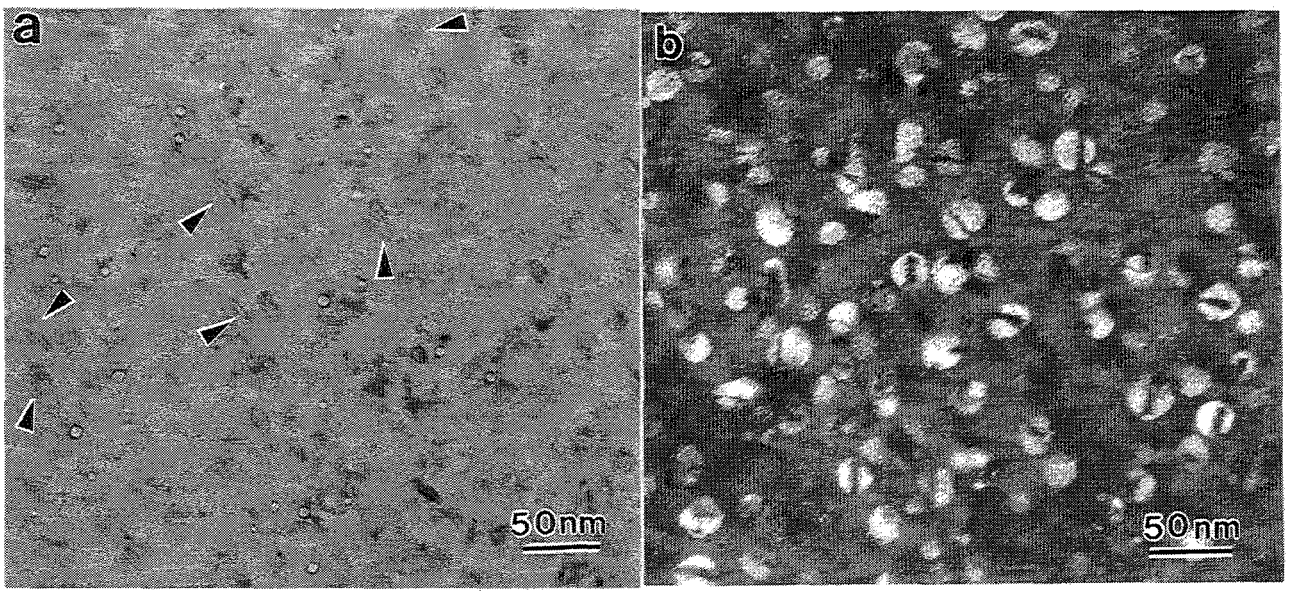

Figure 7. (a) Bright-field TEM micrograph of irradiated Heat A1 which shows the presence of numerous fine cavities and faulted dislocation loops (arrowed). (b) Dark-field TEM micrograph of the faulted γ' precipitates.

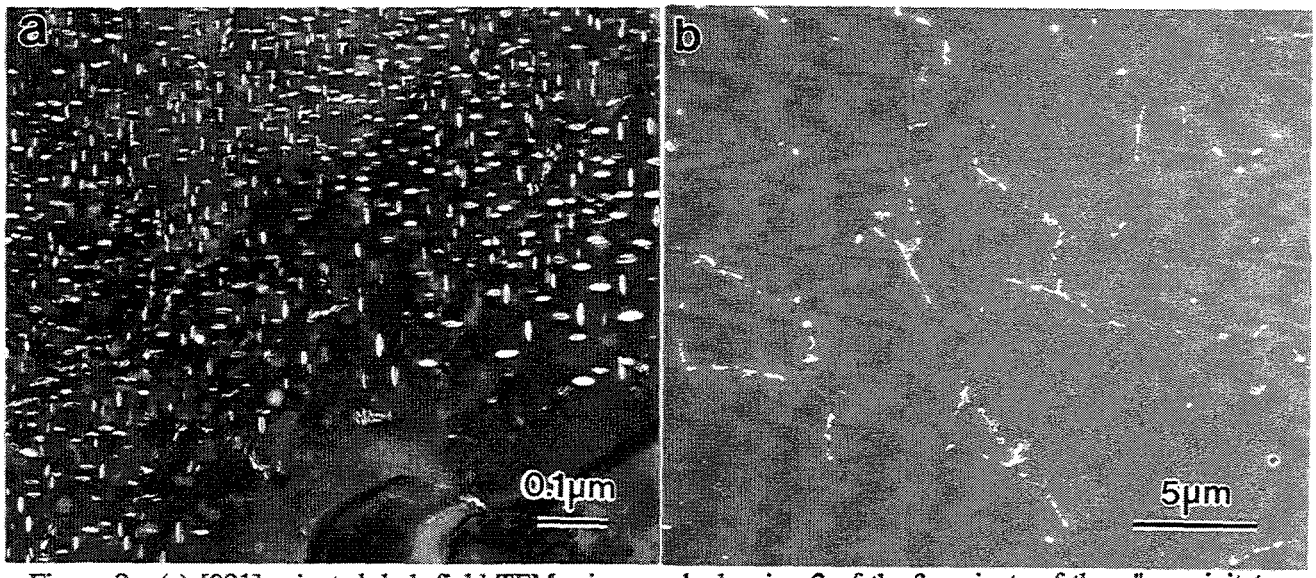

Figure 8. (a) [001]-oriented dark-field TEM micrograph showing 2 of the 3 variants of the γ" precipitates in the vicinity of a PFZ associated with a NbTi-rich inclusion in Alloy 625. Note that the precipitates close to the PFZ are notably coarser than those within the matrix. (b) Secondary electron image of the intergranular carbides in Alloy 625.

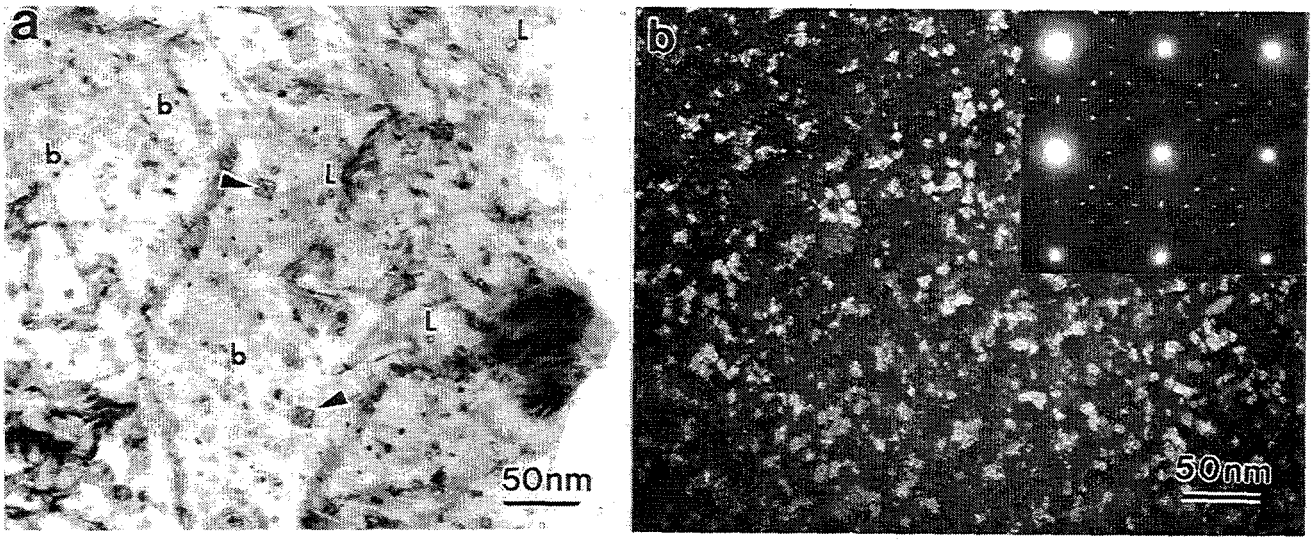

Figure 9. (a) Bright-field TEM image of irradiated Alloy 625 containing "black spot" damage ("b"),fine irradiation-induced dislocation loops ("L"), and stacking fault tetrahedra (arrowed). (b) Dark-field TEM micrograph of the irradiation-induced bco Pt_2Mo-type precipitates and associated [001] diffraction pattern.

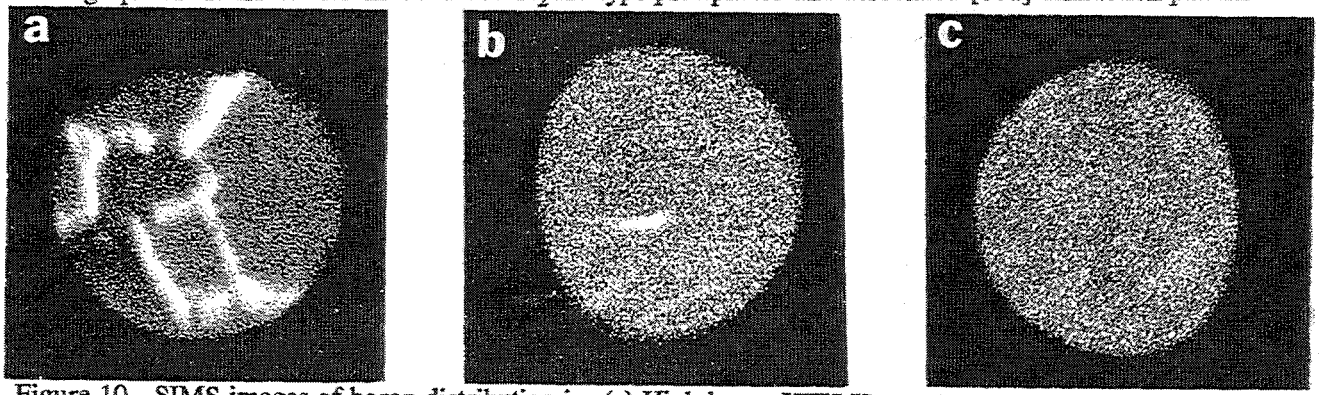

Figure 10. SIMS images of boron distribution in (a) High boron HTH Heat A1, (b) Low boron HTH Heat A7, and (c) Alloy 625. Note that the relative intensity of the peak-to-background signals in (a) is more than an order of magnitude greater than in (b) and (c). Image diameter is approximately 150μm.

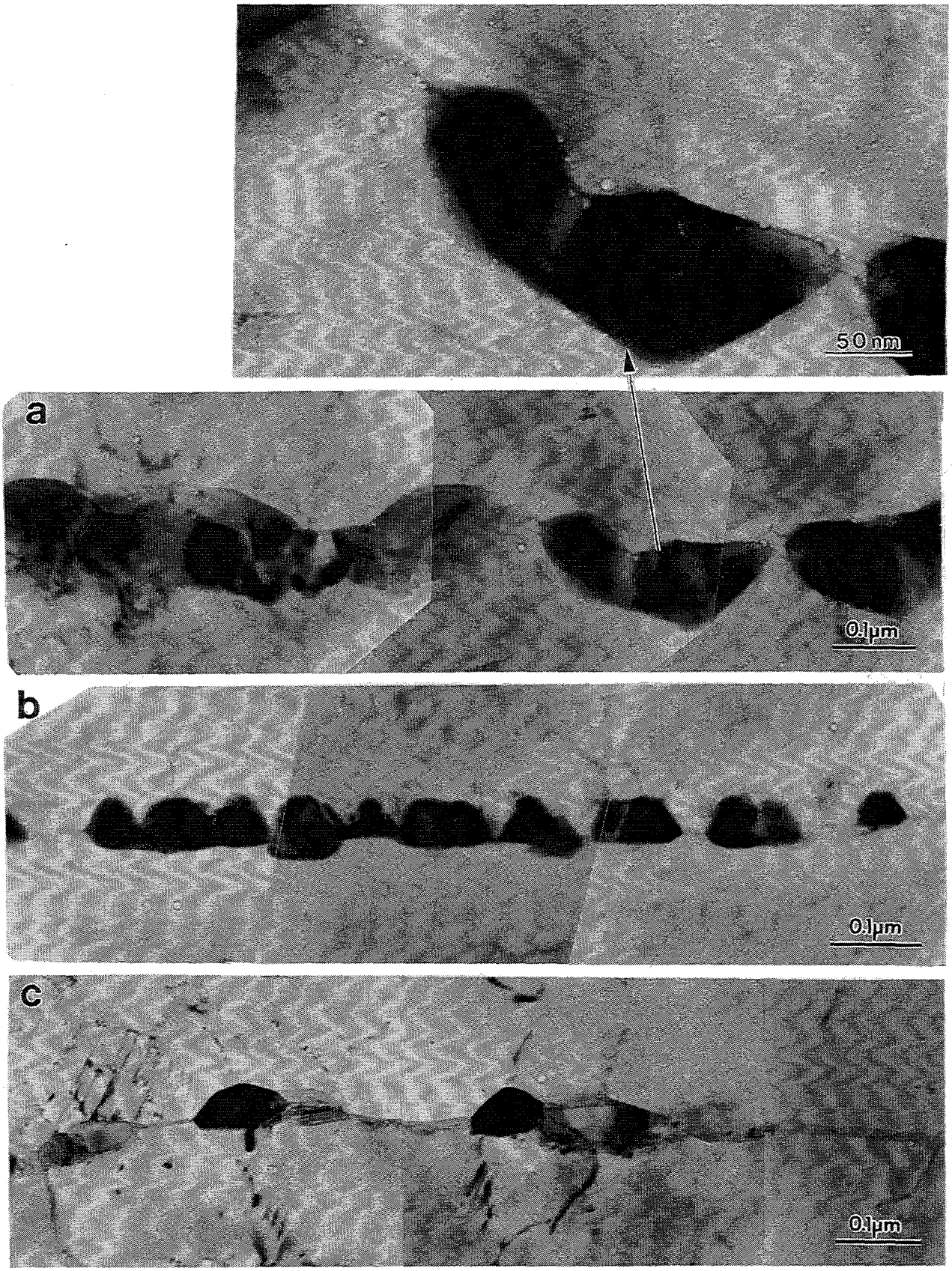

Figure 11. Transmission electron micrographs of irradiated (and annealed), (a) High boron HTH Heat A1, (b) Low boron HTH Heat A7, and (c) Alloy 625. Top micrograph shows enlargement of an area in (a).